Applied Materials Today 21 (2020) 100797

Contents lists available at ScienceDirect

Applied Materials Today

journal homepage: www.elsevier.com/locate/apmt

Metal mesh embedded in colorless shape memory polyimide for flexible transparent electric-heater and actuators

Xinzuo Huang, Fenghua Zhang, Jinsong Leng*

Centre for Composite Materials and Structures, Harbin Institute of Technology (HIT), 150080 Harbin, PR, China

ARTICLE INFO

Article history:
Received 28 May 2020
Revised 27 July 2020
Accepted 14 August 2020

Keywords:
Flexible transparent heater
Actuators
Electro-activated shape memory polymers
Metal mesh
Composites

ABSTRACT

The current electroactive shape memory polymer composites (SMPCs) show low electric heating efficiency, and the transparency of the matrix is seriously damaged by the conductive fillers. In this work, transparent metal mesh is used to replace the conductive fillers to construct a conductive network for electrical actuation for the first time. The self-cracking aluminum mesh is embedded in the transparent shape memory polyimide film (Alm@TSMPI) by solution casting. As a new type of flexible and transparent heater, the Alm@TSMPI has advantages of fast response and high steady-state temperature. As an electric actuator, the Alm@TSMPI is active and deformable depending on its variable stiffness characteristics, and reverts to its original shape within 13 s under electric stimulation. This is the first report on an electroactive transparent shape memory polymer while maintaining light transmission. Moreover, the transition temperature of 230 °C is much higher than that of all other reported electroactive SMPCs. Furthermore, the Alm@TSMPI is attached to transparent shape memory polystyrene as a flexible transparent heater, and the deformation is triggered by electric field. According to this strategy, the Alm@TSMPI can be applied for the electrical actuation of other SMPs, extending the applications in the electric actuators.

1. Introduction

Shape memory polymers (SMPs) can be highly deformed and fixed into a temporary shape under external force. Under the spatially external stimuli, the shape recovery movement can be triggered from temporary shape to the original shape [1,2]. Therefore, SMPs can achieve a variety of designed motions, such as bending, shrinking, twisting [3], *etc*. All the stimuli-responsive movements based on the shape memory effect are programmable. With its special characteristics of low cost, light weight (900–1100 kg/m^3), large deformation (~800%) and easy processing [1], SMPs have been widely applied in various fields, including aerospace engineering [4], biomedical science [5], flexible electronic devices [6]. The external stimulation of environmental change is essential to trigger the programmable movements of SMPs. Heating is the earliest, most common and direct stimulation method. In practical applications, limited by the complexity and particularity of the reality environment, the thermal actuation is often difficult to implement and control. Therefore, indirect, non-contact heating methods have attracted the attention of researchers, such as electrical current, magnetic field and light [1,2].

The applications of polymer actuators with memory and motor ability in artificial muscle [7], biomedical [5] and microfluidic devices [8] have been widely concerned. Electro-activated SMPs are indispensable in polymer actuators, showing advantages of high controllability, easy operation and high efficiency. At present, all reported electro-activated SMP composites are composed of non-conductive SMP matrix and conductive fillers [1]. When an electric field is applied, Joule heat is generated by the conductive fillers dispersed in the polymer matrix. The deformation recovery motion of SMP matrix can be activated when heating above the transition temperature. The applied conductive fillers are divided into two categories: metal particles [9,10] and carbon fillers (e.g. carbon nanotubes [11–24], carbon black [25–29], graphene [30–32], carbon nanofibers [33–35], bucky paper [36–37]). Only when the amount of conductive fillers exceeds a critical value, the continuous conductive network is formed. A large number of conductive fillers make the color of SMP matrix black, completely losing its transparency. However, in the application of flexible electronics and optical devices, the optical transparency of SMPs is absolutely essential [6]. How to realize the electrical actuation of transparent SMPs while ensuring the optical transparency is a huge challenge. In addition, the resistance of SMP composites with conductive fillers is usually large, resulting in low heating power and difficult actuation of the recovery process of SMPs with high transition temperatures above 200 °C. Therefore, it is also an urgent problem

* Corresponding author.
E-mail address: lengjs@hit.edu.cn (J. Leng).

https://doi.org/10.1016/j.apmt.2020.100797
2352-9407/

to make the electro-activated SMPs with high transition temperature.

In this work, transparent metal (Al) mesh embedded on the surface of transparent shape memory polyimide film (TSMPI) is designed. The transparent conductive circuit composed of embedded metal mesh can convert the electric energy into the thermal energy, which makes the active, deformable actuator return to its original shape. This is the first report on electro-activated transparent SMPs with the highest transition temperature (230 °C) compared to other reported electro-activated SMPs. Most importantly, TSMPI embedded with metal mesh can also be applied as an ultra-thin, flexible and transparent heater, and electrical stimulation of any other transparent SMPs can be achieved by attaching the TSMPI heater.

2. Materials and methods

2.1. Materials

Water-based crackle paint was purchased from Guangzhou Day Pulse Chemical Technology Co., Ltd. Both 2,20-bis(trifluoromethyl)−4,40-diaminobiphenyl (TFDB) (98%) and 4,4′-(4,4′-Isopropylidenediphenoxy) diphthalic Anhydride (BPADA) (98%) were purchased from Aladdin LLC.. Chromatographically pure dimethylacetamide (DMAc) was purchased from Tianjin Guangfu Fine Chemicals Institute. All chemical reagents were used in the experiments directly without further treatment.

2.2. Sample preparation

The initial viscosity of water-based crackle paint was 2.9 Pa•s at 25 °C, then the viscosity was diluted to 1.2 Pa•s by deionized water. The diluted crackle paint was spin-coated on the surface of the glass substrate, at 25 °C. The rotation speed was 1500 rpm, and the spin coating time was 15 s. The self-cracking template was converted by drying the paint film in a constant temperature and humidity oven, at 25 °C with the humidity of 25%RH. The designed mask and self-cracking template were placed in vacuum evaporator (ZHDS400, Beijing Technol Science Co., Ltd.). A patterned aluminum film was deposited on the crack template surface using high purity aluminum particles (99.99%) as evaporation source. The vacuum degree was less than 5×10^{-4} Pa, and the evaporation rate and time was 0.8~1.0 nm/s and 6 min. The deposited substrate was ultrasonically cleaned in 70 °C DMAc for 60 s, and the self-cracking template was removed. The patterned Al mesh raised on the glass substrate was manufactured after the crack template peeled off.

The schematic diagram of synthesis of TSMPI can refer to our previous work [38]. The polyamic acid solution was obtained by mixing TFDB (1.9 mmol), BPADA (2.0 mmol) and DMAc (10 ml) in the flask and stirring at room temperature for 20 h. The polyamic acid solution was casted onto the glass with Al mesh on the surface. The step-wise imidization curing process (80~300 °C) was carried out, and the patterned Al mesh embedded in TSMPI was finally prepared. The average thickness of TSMPI film with 70 μm was controlled by adjusting the volume of polyamic acid solution per unit area. The transparent shape memory polystyrene sheet (30×9*2 mm) was prepared according to the reference [39].

2.3. Characterization

The viscosity of the water-based crackle paint was measured by a rotary rheometer (TA Instruments, DHR-2) at 25 °C and at a shear rate of 3.0 1/s. The micro morphology was characterized by laser confocal microscope (LCM, Olympus OLS5000) and optical digital microscope (Keyence, VHX-900) at room temperature. Scanning electron microscopy (SEM) was performed on a Zeiss Sigma300 instrument at an accelerating voltage of 5 kV. The optical transmittance (200~800 nm) was measured by a Perkin Elmer Lambda 1050 UV/Vis/NIR spectrophotometer at the resolution of 1 nm. The value of three different samples was used in the transmittance test. The sheet resistance (R_s) was evaluated by four-point probe measurement (NAPSON, RG-7C) at room temperature. The thermomechanical properties of polymer were characterized by dynamic mechanical analysis (DMA) (TA Instruments Q800), under the tensile mode with a frequency of 1 Hz, at a heating rate of 3 °C min^{-1}. The transient surface temperature field of the flexible transparent heater was measured by an infrared thermal image instrument. The strip sample (angle 180°) was folded to an angle 0° under heating, and the temporary shape was fixed by cooling down to room temperature under the action of external force. Then the external force was removed and the fixed angle (θ_f) of the sample was determined. The shape fixity ratio (R_f) can be expressed as Eq. (1). In the shape recovery experiment, the temporary shape was heated in an electric field, from which the recovery angle θ_r was recorded. The shape recovery ratio (R_r) was calculated according to Eq. (2). The average values of the R_f and R_r were acquired by three consecutive bending-recovery shape memory cycle tests.

$$R_f = \frac{180 - \theta_f}{180} \times 100\% \quad (1)$$

$$R_t = \frac{\theta_r - \theta_f}{180 - \theta_f} \times 100\% \quad (2)$$

3. Results and discussions

Fig. 1 shows the preparation process of transparent shape memory polyimide film embedded with metal mesh on the surface. Firstly, a fast and low-cost technology was used to prepare Al mesh on the glass substrate. A uniform micro-crack template was obtained by coating self-cracking water-based crackle paint on the glass substrate. The Al film with low-cost, good oxidation resistance and good conductivity was deposited on the crack template by vacuum thermal evaporation. The crack template was rapidly peeled off from the glass surface by ultrasonic cleaning, while the Al mesh remained on the glass surface (Alm@glass). Secondly, the precursor of polyimide, polyamide acid solution, was synthesized according to the previous research [38]. The polyamide acid solution was coated on the glass surface with metal mesh by solution casting. The polyimide film was prepared through imidization reaction after staged heating. Finally, the Al mesh on the glass surface was peeled off and embedded in the transparent shape memory polyimide (Alm@TSMPI). The combination of Al atoms and glass substrate is dominated by the weak van-der waals force. The adhesion between Al mesh and glass substrate is very weak. Due to the high modulus and size shrinkage of cured polymer, TSMPI substrate exerts a strong Von-Mises stress on the embedded Al mesh, which is far more than the adhesion force between Al mesh and glass substrate. Therefore, during the peel-off process, the Al mesh on the glass substrate can be transferred to the surface of TSMPI substrate without defects during the stripping process.

The millimeter-scale cracks produced by water-based crackle paint are commonly used in surface decoration of handcrafts and buildings. During the drying process, the film cracks due to the concentration of internal stress [40]. Under the condition of stable temperature and humidity, different film thicknesses lead to different water loss rates and internal stress states, and ultimately cause different crack morphologies. With the increase of the film thickness, the crack width of the mesh template becomes wider, and the mesh size becomes inhomogenous [41]. Under the constant viscosity (~1.2 Pa•s), the faster the spin-coating speed, the thinner the paint film thickness. By adjusting the spin-coating speed

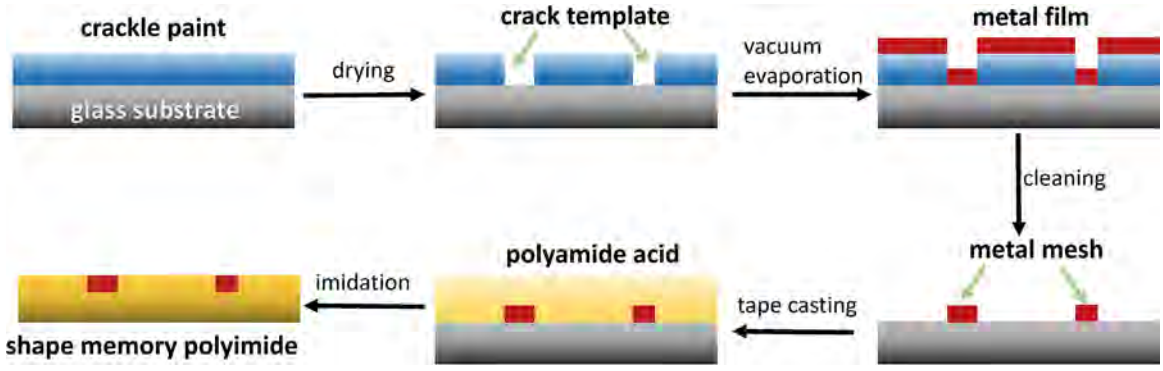

Fig. 1. Manufacturing process of transparent shape memory polyimide film with embedded metal mesh.

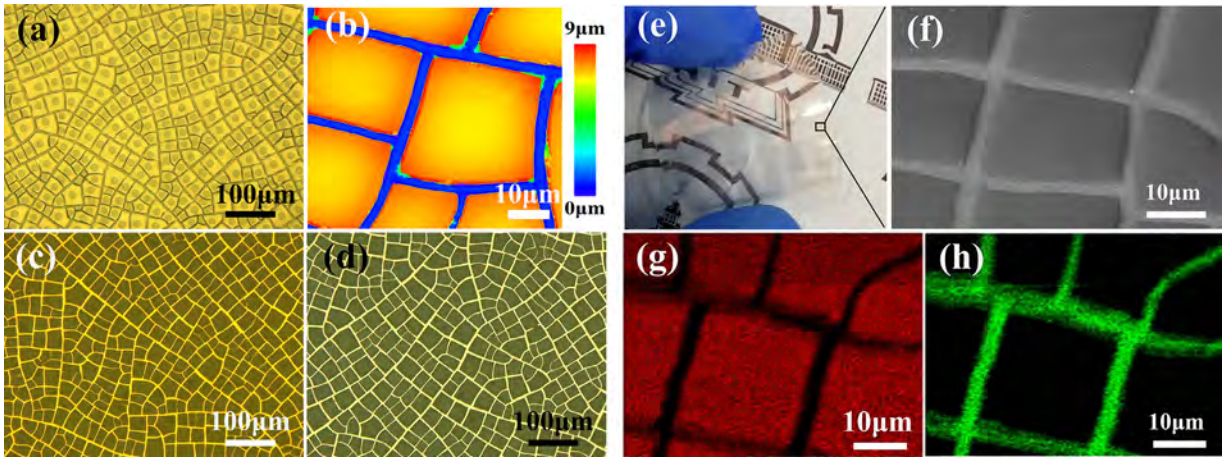

Fig. 2. (a) Optical microscope and (b) laser confocal microscope image of micro-crack template. Optical microscope image of metal mesh (c) on glass substrate and (d) embedded in polyimide substrate. (e) Digital photo of TSMPI film with patterned transparent conductive circuit. (f) SEM image of metal mesh embedded in polyimide substrate. EDS mapping of (g) C element and (h) Al element on the Alm@TSMPI.

(1500 rpm) to form a paint film with appropriate thickness, a micrometer-scale crack template is obtained, as shown in Fig. 2a. The template is mainly composed of a large number of quadrilateral microcracks with similar geometry. Through controlling the morphology of microcracks, a suitable micro-crack template is prepared, and the cracks are concentrated in the width distribution. The results show that the crack width ranges from 2 to 6 μm, with an average value of 4.0 $\pm$ 1.2 μm. Fig. 2b is a laser confocal microscope image of the micro-crack template. It is intuitively observed that the thickness of micro-crack template is uniform, and the crack depth is about 6.5 μm. The optical microscope image of the Alm@glass produced by vacuum evaporation and ultrasonic cleaning is shown in Fig. 2c. There is no damage or fracture appearing on the Al mesh during the template removal process. The morphology of the metal mesh is completely copied from the macro-crack template (Fig. 2a).

Fig. 2d is an optical microscope image of the metal mesh embedded in the polyimide substrate. In the process of TSMPI curing and demolding, the metal mesh still remains intact during the transition from rigid structure to flexible structure. When designing a mask in vacuum evaporation, the metal mesh can be patterned to produce transparent conductive circuits of any shape. As shown in Fig. 2e, a slightly darker U-shaped transparent conductive circuit is distributed on the surface of colorless shape memory polyimide. Fig. 2f shows the SEM image of the Alm@TSMPI, revealing that the width of the Al meshes ranges from 2 to 6 μm, similar to the optical microscope result. Energy dispersive spectrometer (EDS) mapping of the Alm@TSMPI is shown in Fig. 2g and h. The red part in Fig. 2g represents carbon element, which proves that the region is polyimide substrate. In Fig. 2h, the green part and the red part complement each other to represent the aluminum element, which proves that the mesh area is metallic aluminum. The raised shadow on the interface reveals that the metal mesh is embedded in the polyimide, rather than simply on the surface (Fig. 2f). In addition, the Alm@TSMPI has the advantages of flexible durability, ultra-low surface roughness and strong adhesion due to this unique embedded structure [41].

The conductive circuit embedded with transparent metal mesh in TSMPI has a broad application prospect in flexible transparent film heaters. For the heater based on Joule heating effect, the resistance is an important parameter affecting heating power. At the same voltage, the lower the resistance, the higher the conversion rate of electric energy to thermal energy. The average square resistance (R_s) of the Alm@TSMPI film heater adopted by four-point probe method is 3.0 Ω sq^{-1}. Fig. 3a shows the electrothermal performance of the Alm@TSMPI heater at different applied voltages. When the power is turned on, the surface temperature rises rapidly and reaches the steady-state temperature within a few seconds. Once the power is cut off, the surface temperature drops rapidly to room temperature. The higher the applied voltage, the higher the steady-state temperature. The time from room temperature to the steady-state temperature is defined as the response time of heaters. When the applied voltage is 6 V and 12 V, the Alm@TSMPI can reach the steady-state temperatures of 95 °C and 235 °C in the response time of 20 s. Fig. 3b shows the temperature versus power density plot of the Alm@TSMPI. With the increase of power density, the steady-state temperature increases linearly. By calculating the slope of the fitted curve in Fig. 3b, the thermal

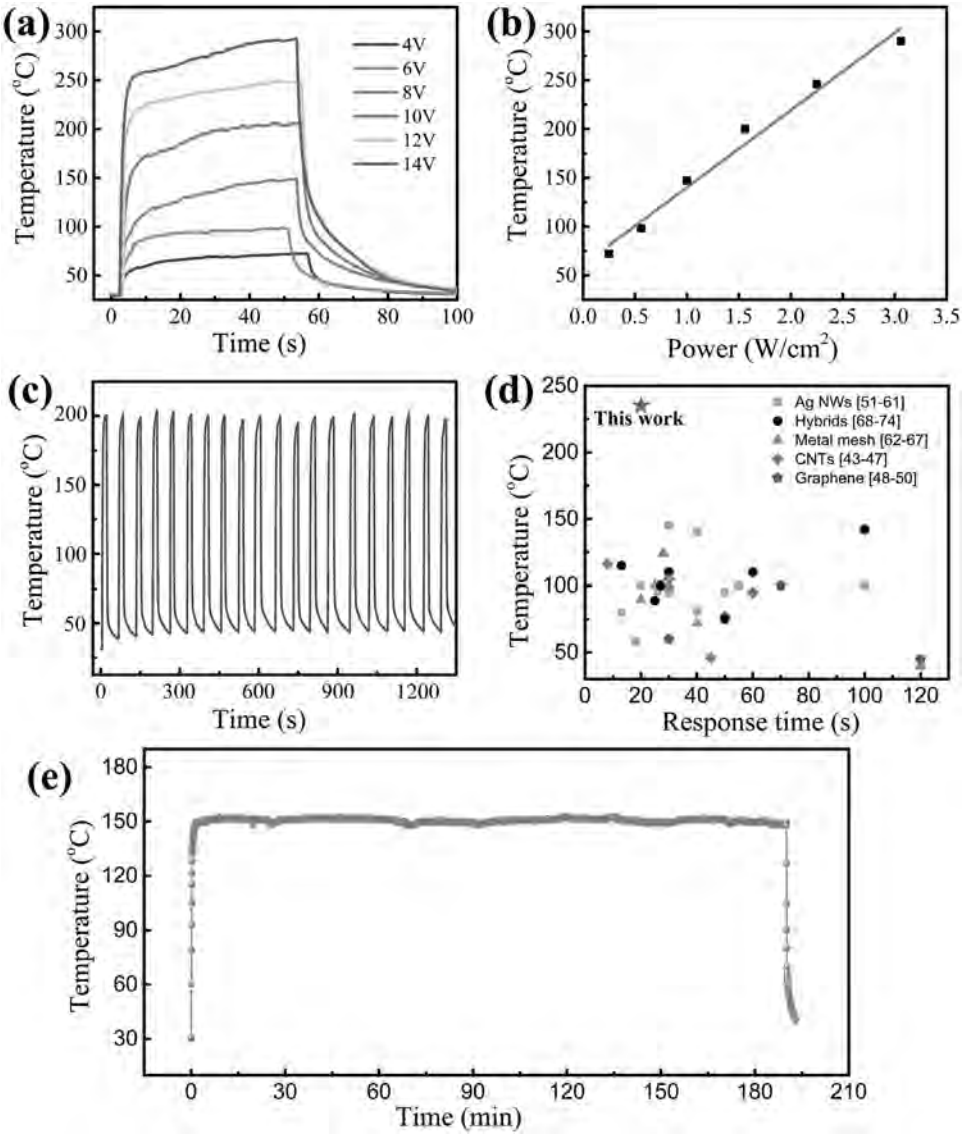

Fig. 3. (a) Time-dependent temperature profiles of the Alm@TSMPI (actual conductive area~200 mm^2) at different applied voltages (R_s=3.0 Ω sq^{-1}). (b) Temperature versus power density plot of the Alm@TSMPI transparent heater. (c) Switching thermal stability cycles of the Alm@TSMPI transparent heater with 0 and 10 V applied voltages. (d) The steady-state temperature versus response time of the Alm@TSMPI film heater compared to the results of literature. (e) Temperature variation at an applied voltage of 8 V for 3 h.

resistance and electrical power consumption of the Alm@TSMPI heater are approximately 79.2 °C W^{-1} cm^2.

The cyclic thermal stability of the Alm@TSMPI heater is further measured by switching the input power voltage from 0 to 10 V (Fig. 3c). The results of 20 heating and cooling cycles show that the Alm@TSMPI has sufficient thermal stability. The steady-state temperature and the response time are the key indicators to evaluate the electrothermal performance of heaters. Flexible transparent heaters have the advantages of high steady-state temperature and fast response speed. It has been widely applied in the fields of defogging and defrosting windows, wearable electronic equipment, thermal sensors and other fields [42]. The Alm@TSMPI heater with the steady-state temperature of 235 °C and the response time of 20 s is superior to other reported flexible transparent heaters based on carbon nanotubes (CNTs) [43–47], graphene [48–50], silver nanowires (AgNWs) [51–61], metal mesh [62–67] and their hybrids [68–74] (Fig. 3d). The AgNWs network is easy to melt and fracture at high temperature, which limits the maximum steady-state temperature of AgNWs based heaters (<160 °C) [54]. CNTs and graphene-based heaters are generally less electrothermal efficient because of their high resistance. The upper limit of steady-state temperature of metal mesh based heater is determined by the thermal resistance of substrate material. In this work, shape memory polyimide as the flexible transparent heater substrate has excellent heat resistance, greatly increasing the upper limit of steady-state temperature. The Al crack network shows high interconnectivity and non-contact resistance, which can efficiently convert electrical energy into thermal energy. Therefore, the flexible transparent heater based on metal mesh has the characteristics of fast response and high steady-state temperature. Ye et al. demonstrated that the response time of transparent electric-heater could be prolonged as the glass substrate thickness increases 30 times [69]. As shown in Fig. 3d, we found that more than half of literatures on flexible transparent heaters did not point out the thickness of the flexible substrate. The effective thickness of the polymer substrates was statistically varied from 50 to 150 μm. The thickness of TSMPI used in this work is about 70 μm. Considering that the difference in the thickness of each polymer substrate is relatively

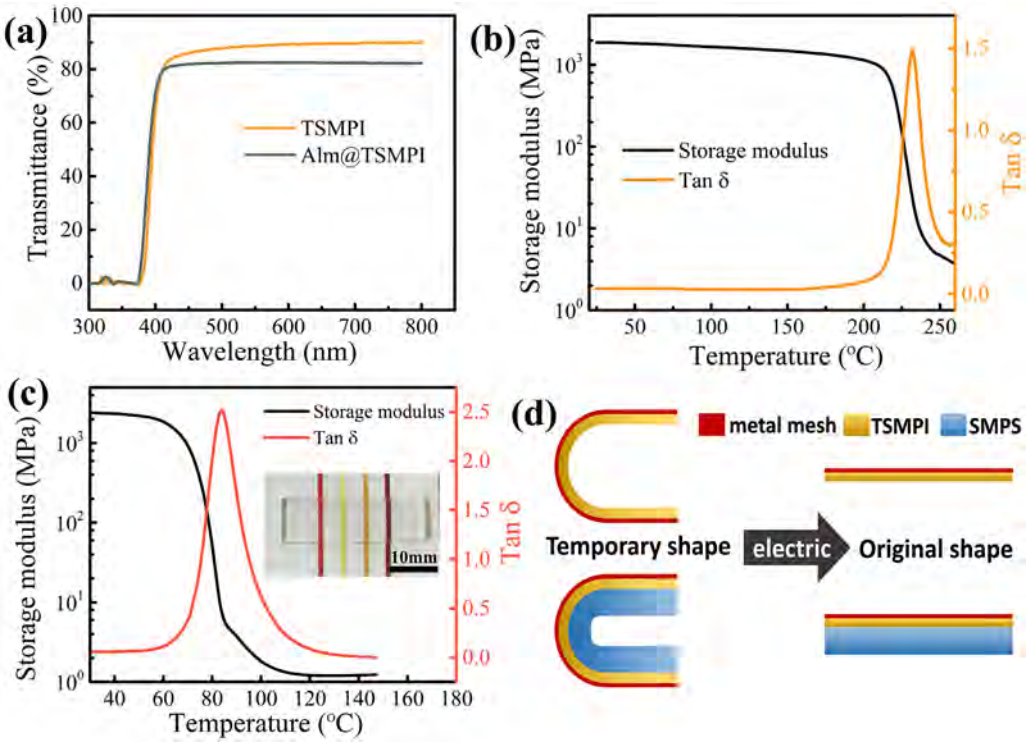

Fig. 4. (a) UV–vis spectra of TSMPI substrate and flexible transparent heater (Alm@TSMPI). Dynamic mechanical analysis results of (b) TSMPI and (c) Shape memory polystyrene, the insert picture is the digital photo of transparent polystyrene. (d) Schematic diagram of metal mesh for electrical stimulation of transparent shape memory polymers.

small, the effect of substrate thickness on the response time is temporarily ignored in Fig. 3d. Furthermore, the long-term heating stability was also demonstrated by long-term loading applied voltage (8 V). Fig. 3e shows that there is no temperature fluctuation in the Alm@TSMPI which works continuously for 3 h under the steady-state temperature of 150 °C. Therefore, the Alm@TSMPI heater could easily satisfy the reliability requirements of flexible transparent heaters in most applications. This excellent long-term heating stability may benefit from the protection of the polymer substrate on the embedded Al mesh.

The light transmittance of the flexible transparent heater in the visible light range is shown in Fig. 4a. The transmittance of transparent shape memory polyimide substrate at 550 nm (T_{550}) is around 90%. The strongly electron-withdrawing and bulky -CF_3 inhibit the formation of charge transfer complexes, which determines that TSMPI film has excellent optical transparency [33]. The metal mesh embedded in TSMPI as an obstacle can block the penetration of visible light, thus the T_{550} of the Alm@TSMPI is reduced to 83%. The thermomechanical properties of SMPs are shown in Fig. 4b and c. The peak value of loss factor (Tan δ) represents the glass transition temperature (T_g) of polymer. Fig. 4b shows that TSMPI has a T_g of 230 °C, which is much higher than other transparent SMPs and has excellent heat resistance. Therefore, TSMPI based flexible transparent heater can be applied in high temperature environment, which greatly expands potential applications. Shape memory polystyrene (SMPS) exhibited good shape memory performance, adjustable transition temperature (60~85 °C) [39], and, excellent optical transparency. The transmittance of SMPS in visible spectrum is 95% [75]. In this work, we use the electrical stimulation of another SMPs as an example to demonstrate the Alm@TSMPI. The T_g of transparent SMPS is about 83 °C, and the inset image in Fig. 4c shows the high optical transparency of SMPS. When the polymer transferring from glassy state to rubber state at transition temperature, the storage modulus decreases in geometrically (Fig. 4b~c), which provides shape memory effect for TSMPI and SMPS. The networks in SMPs are composed of macromolecular chain segments and network points. The netpoints link the macromolecular chain segments together, which remain stable and determine the original shape of the polymer [3]. The physical crosslinking formed by intermolecular interactions is the netpoints of TSMPI. The netpoints in transparent SMPS are generated by covalent bonds (chemical crosslinking).

Fig. 4d is the schematic diagram of the metal mesh for electrical stimulation of transparent shape memory polymers. In the programming process of shape memory effect, the rectangular Alm@TSMPI (angle 180°) is folded into angle 0° under the action of heating and external force, and the temporary shape is memorized when removing the heat and force. Under the appropriate voltage, the Joule heat generated by the current is transmitted to the TSMPI substrate through the transparent conductive circuit composed of metal meshes. When the temperature rises to T_g, the recovery movement from the temporary shape to the original shape is triggered. As an ultra-thin, flexible and transparent heater, the Alm@TSMPI with a thickness of only 70 μm is pasted on the transparent SMPS. With the bending deformation of SMPS, the Alm@TSMPI has the same non-interference deformation. Similarly, the Joule heat generated by the Alm@TSMPI can activate SMPS at lower voltage.

Fig. 5a shows the shape memory recovery process of the Alm@TSMPI film under electrical stimulation. The infrared thermal image corresponding to Fig. 5a is shown in Fig. 5b. According to the electrical heating characteristic curve (Fig. 3a), the heat generated at 12 V is sufficient to trigger the recovery of TSMPI (T_g=230 °C). The rapid thermal conductivity is present as a result of the ultrathin thickness. Within 1.5 s after power-on, the metal mesh quickly heats the TSMPI substrate to drive the recovery motion. The Alm@TSMPI has superfast response and recovery speed, and its temporary shape returns to its original shape within 13 s.

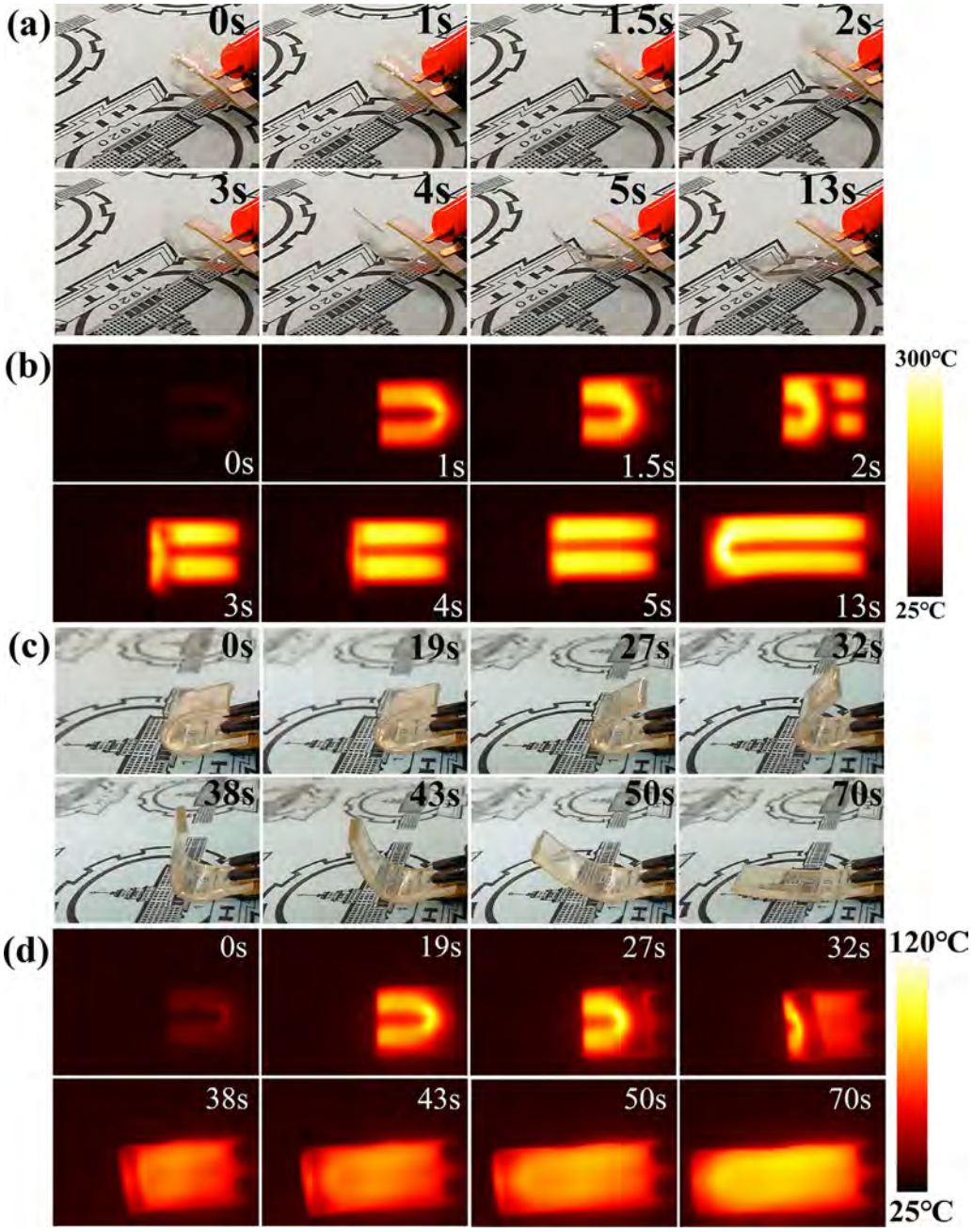

Fig. 5. (a) Digital photos and (b) infrared thermal images of shape memory recovery process of the Alm@TSMPI at 12 V DC. (c) Digital photos and (d) infrared thermal images of shape memory recovery process of transparent SMPS at 6 V DC.

Fig. 5c shows the shape recovery process of transparent SMPS under electrical stimulation. The infrared thermal image corresponding to Fig. 5c is shown in Fig. 5d. SMPS slice (30×9*2 mm) and the Alm@TSMPI film are stuck together by a transparent 3 M double-sided tape. Low voltage of 6 V is adopted to trigger shape memory recovery of SMPS due to its low transition temperature of 83 °C. After power on, the transparent SMPS is triggered to recover after 19 s, and the whole recover process takes 70 s. The response speed and the recovery speed of electro-activated SMPS are much slower than that of the Alm@TSMPI. Because the thickness of SMPS slice is much larger than that of TSMPI film, it takes a long time to transfer heat from one side to the other side. At the end of recovery, the average temperature of the instantaneous surface temperature field reaches 90 °C. Shape fixity ratio (R_f) and shape recovery ratio (R_r) are two important characteristic parameters of shape memory materials. The shape memory properties of electro-activated SMPs are measured by bending deformation method. For specific test details, see the characterization section. Electro-activated SMPs with flexible metal mesh as transparent heater can obtain excellent shape memory performance. The R_f and R_r of Alm@TSMPI are 99% and 96%, respectively. Under electrical stimulation, the R_f and R_r of transparent SMPS are 99% and 98%, respectively.

Compared with other reported literatures, the results of shape recovery process under electrical stimulation are shown in Fig. 6. All the reported electro-activated SMPs are prepared by adding conductive particles in polymer matrix, such as CNTs, carbon nanofibers (CNFs), carbon black (CB), nickel nanoparticles (NiPs). The doping of conductive fillers in SMP matrix is random, resulting in well-distributed heat transfer in the thickness direction. Therefore, in Fig. 6, the effect of matrix thickness on the shape recov-

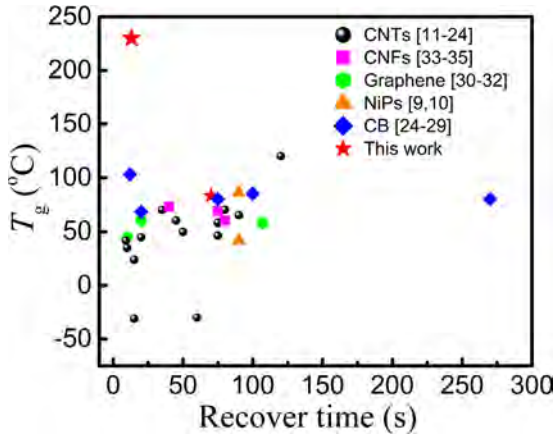

Fig. 6. The transition temperature versus shape memory recover time of this work compared to the literature results.

ery time of electro-activated SMPs can be ignored. This strategy of building conductive networks with fillers has two disadvantages. The composites with fillers have high resistivity and low electrical heating power. It is difficult to achieve shape recovery of SMPs with high transition temperatures (>150 °C) by electrical heating. Most importantly, no matter what kind of conductive filler is added, the transparency of transparent SMPs can be destroyed. In this work, the conductive network is constructed by embedded metal mesh rather than conductive fillers. It not only realizes the fast electro-activated recovery (13 s) of TSMPI with high transition temperature (230 °C), but also maintains its high light transmission.

4. Conclusions

In summary, the metal (Al) mesh embedded in transparent shape memory polyimide film (TSMPI) is fabricated via self-cracking template and solution-coating. The transmittance of Alm@TSMPI at 550 nm is 83%, and the sheet resistance is 3.0 Ω sq^{-1}. The Alm@TSMPI has the advantages of fast response and high steady-state temperature, which reach the steady-state temperatures of 235 °C in the response time of 20 s. Depending on the shape memory effect of polymer substrate, the Alm@TSMPI is an active, deformable, electric actuator that can recover its original shape within 13 s under electric stimulation. TSMPI has the highest transition temperature (230 °C) among all the reported electroactive shape memory polymers. In addition, not limited to transparent SMPs, the electrical response of all SMPs with transition temperature below 230 °C can be achieved by attaching the Alm@TSMPI flexible transparent heater. It is of great significance to extend the application of flexible transparent actuators.

Declaration of Competing Interest

The authors declare that they have no known competing financial interests or personal relationships that could have appeared to influence the work reported in this paper.

CRediT authorship contribution statement

Xinzuo Huang: Conceptualization, Methodology, Investigation, Writing - original draft. **Fenghua Zhang:** Writing - review & editing, Project administration. **Jinsong Leng:** Resources, Supervision, Funding acquisition.

Acknowledgments

This work was supported by the National Natural Science Foundation of China (Grant Nos: 11632005).

References

[1] T. Liu, T. Zhou, Y. Yao, F. Zhang, L. Liu, Y. Liu, J. Leng, Stimulus methods of multi-functional shape memory polymer nanocomposites: a review, Compos. Pt. A-Appl. Sci. Manuf. 100 (2017) 20–30.
[2] W. Wang, Y. Liu, J. Leng, Recent developments in shape memory polymer nanocomposites: actuation methods and mechanisms, Coord. Chem. Rev. 320-321 (2016) 38–52.
[3] A. Lendlein, O.E.C. Gould, Reprogrammable recovery and actuation behaviour of shape-memory polymers, Nat. Rev. Mater. 4 (2019) 116–133.
[4] L. Santo, F. Quadrini, A. Accettura, W. Villadei, Shape memory composites for self-deployable structures in aerospace applications, Procedia Eng. 88 (2014) 42–47.
[5] A. Kirillova, L. Ionov, Shape-changing polymers for biomedical applications, J. Mat. Chem. B 7 (2019) 1597–1624.
[6] H. Gao, J. Li, F. Zhang, Y. Liu, J. Leng, The research status and challenges of shape memory polymer-based flexible electronics, Mater. Horiz. 6 (2019) 931–944.
[7] A. Khaldi, J.A. Elliott, S.K. Smoukov, Electro-mechanical actuator with muscle memory, J. Mater. Chem. C 2 (2014) 8029–8034.
[8] W. Hilber, Stimulus-active polymer actuators for next-generation microfluidic devices, Appl. Phys. A-Mater. Sci. Process. 122 (2016) 751.
[9] H. Lu, F. Liang, J. Gou, Nanopaper enabled shape-memory nanocomposite with vertically aligned nickel nanostrand: controlled synthesis and electrical actuation, Soft Matter 7 (2011) 7416–7423.
[10] J.S. Leng, X. Lan, Y.J. Liu, S.Y. Du, W.M. Huang, N. Liu, S.J. Phee, Q. Yuan, Electrical conductivity of thermoresponsive shape-memory polymer with embedded micron sized Ni powder chains, Appl. Phys. Lett. 92 (2008) 014104.
[11] S. Raghunath, S. Kumar, S.K. Samal, S. Mohanty, S.K. Nayak, PLA/ESO/MWCNT nanocomposite: a study on mechanical, thermal and electroactive shape memory properties, J. Polym. Res. 25 (2018) 126.
[12] T. Liu, R. Huang, X. Qi, P. Dong, Q. Fu, Facile preparation of rapidly electro-active shape memory thermoplastic polyurethane/polylactide blends via phase morphology control and incorporation of conductive fillers, Polymer 114 (2017) 28–35.
[13] J. Chen, Z. Zhang, W. Huang, J. Li, J. Yang, Y. Wang, Z. Zhou, J. Zhang, Carbon nanotube network structure induced strain sensitivity and shape memory behavior changes of thermoplastic polyurethane, Mater. Des. 69 (2015) 105–113.
[14] F. Du, E. Ye, W. Yang, T. Shen, C. Tang, X. Xie, X. Zhou, W. Law, Electroactive shape memory polymer based on optimized multi-walled carbon nanotubes/polyvinyl alcohol nanocomposites, Compos. Pt. B-Eng. 68 (2015) 170–175.
[15] S.S. Mahapatra, S.K. Yadav, H.J. Yoo, M.S. Ramasamy, J.W. Cho, Tailored and strong electro-responsive shape memory actuation in carbon nanotube-reinforced hyperbranched polyurethane composites, Sens. Actuators B 193 (2014) 384–390.
[16] M. Raja, S.H. Ryu, A.M. Shanmugharaj, Influence of surface modified multi-walled carbon nanotubes on the mechanical and electroactive shape memory properties of polyurethane (PU)/poly(vinylidene diflouride) (PVDF) composites, Colloid Surf. A-Physicochem. Eng. Asp. 450 (2014) 59–66.
[17] J. Alam, M. Alam, M. Raja, Z. Abduljaleel, L.A Dass, MWCNTs-reinforced epoxidized linseed oil plasticized polylactic acid nanocomposite and its electroactive shape memory behaviour, Int. J. Mol. Sci. 15 (2014) 19924–19937.
[18] M. Raja, S.H. Ryu, A.M. Shanmugharaj, Thermal, mechanical and electroactive shape memory properties of polyurethane (PU)/poly (lactic acid) (PLA)/CNT nanocomposites, Eur. Polym. J. 49 (2013) 3492–3500.
[19] G. Fei, G. Li, L. Wu, H. Xia, A spatially and temporally controlled shape memory process for electrically conductive polymer-carbon nanotube composites, Soft Matter 8 (2012) 5123.
[20] Y.C. Jung, H.J. Yoo, Y.A. Kim, J.W. Cho, M. Endo, Electroactive shape memory performance of polyurethane composite having homogeneously dispersed and covalently crosslinked carbon nanotubes, Carbon 48 (2010) 1598–1603.
[21] N.G. Sahoo, Y.C. Jung, J.W. Cho, Electroactive shape memory effect of polyurethane composites filled with carbon nanotubes and conducting polymer, Mater. Manuf. Process. 22 (2007) 419–423.
[22] J.W. Cho, J.W. Kim, Y.C. Jung, N.S. Goo, Electroactive shape-memory polyurethane composites incorporating carbon nanotubes, Macromol. Rapid. Commun. 26 (2005) 412–416.
[23] Z. Wang, J. Zhao, M. Chen, M. Yang, L. Tang, Z. Dang, F. Chen, M. Huang, X. Dong, Dually actuated triple shape memory polymers of cross-linked polycyclooctene-carbon nanotube/polyethylene nanocomposites, ACS Appl. Mater. Interfaces 6 (2014) 20051–20059.
[24] Y. Liu, F. Zhang, J. Leng, K. Fu, X.L. Lu, L. Wang, C. Cotton, B. Sun, B. Gu, T. Chou, Remotely and sequentially controlled actuation of electroactivated carbon nanotube/shape memory polymer composites, Adv. Mater. Technol. 4 (2019) 1900600.
[25] K. Yu, Z. Zhang, Y. Liu, J. Leng, Carbon nanotube chains in a shape memory polymer/carbon black composite: to significantly reduce the electrical resistivity, Appl. Phys. Lett. 98 (2011) 074102.

[26] K. Wei, G. Zhu, Y. Tang, X. Li, Electroactive shape-memory effects of hydro-epoxy/carbon black composites, Polym. J. 45 (2013) 671–675.
[27] T. Ren, G. Zhu, Y. Liu, X. Hou, An investigation on electro-induced shape memory performances of CE/EP/CB/SCF composites applied for deployable structure, J. Polym. Eng. 40 (2020) 203–210.
[28] J. Du, Z. Zhang, D. Liu, T. Ren, D. Wan, H. Pu, Triple-stimuli responsive shape memory effect of novel polyolefin elastomer/lauric acid/carbon black nanocomposites, Compos. Sci. Technol. 169 (2019) 45–51.
[29] Y. Wei, R. Huang, P. Dong, X. Qi, Q. Fu, Preparation of polylactide/poly(ether)urethane blends with excellent electro-actuated shape memory via incorporating carbon black and carbon nanotubes hybrids fillers, Chin. J. Polym. Sci. 36 (2018) 1175–1186.
[30] L. Valentini, M. Cardinali, J. Kenny, Hot press transferring of graphene nanoplatelets on polyurethane block copolymers film for electroactive shape memory devices, J. Polym. Sci. Part B 52 (2014) 1100–1106.
[31] S. Rana, J.W. Cho, L.P. Tan, Graphene-crosslinked polyurethane block copolymer nanocomposites with enhanced mechanical, electrical, and shape memory properties, RSC Adv. 3 (2013) 13796–13803.
[32] E. D'Elia, H.S. Ahmed, E. Feilden, E. Saiz, Electrically-responsive graphene-based shape-memory composites, Appl. Mater. Today 15 (2019) 185–191.
[33] H. Lu, W. Yin, W.M. Huang, J. Leng, Self-assembled carboxylic acid-functionalized carbon nanotubes grafting onto carbon fiber for significantly improving electrical actuation of shape memory polymers, RSC Adv. 3 (2013) 21484–21488.
[34] H. Lu, F. Liang, Y. Yao, J. Gou, D. Hui, Self-assembled multi-layered carbon nanofiber nanopaper for significantly improving electrical actuation of shape memory polymer nanocomposite, Compos. Pt. B-Eng. 59 (2014) 191–195.
[35] C. Zeng, L. Liu, W. Bian, Y. Liu, J. Leng, 4D printed electro-induced continuous carbon fiber reinforced shape memory polymer composites with excellent bending resistance, Compos. Pt. B-Eng. 194 (2020) 108034.
[36] W. Wang, D. Liu, Y. Liu, J. Leng, D. Bhattacharyya, Electrical actuation properties of reduced graphene oxide paper/epoxy-based shape memory composites, Compos. Sci. Technol. 106 (2015) 20–24.
[37] H. Lu, W.M. Huang, J. Leng, Functionally graded and self-assembled carbon nanofiber and boron nitride in nanopaper for electrical actuation of shape memory nanocomposites, Compos. Pt. B-Eng. 62 (2014) 1–4.
[38] X. Huang, F. Zhang, Y. Liu, J. Leng, Flexible and colorless shape memory polyimide films with high visible light transmittance and high transition temperature, Smart Mater. Struct. 28 (2019) 055031.
[39] D. Zhang, Y. Liu, K. Yu, J. Leng, Influence of cross-linking agent on thermomechanical properties and shape memory effect of styrene shape memory polymer, J. Intell. Mater. Syst. Struct. 22 (2011) 2147–2154.
[40] W.P. Lee, A.F. Routh, Why do drying films crack? Langmuir 20 (2004) 9885–9888.
[41] X. Huang, F. Zhang, Y. Liu, J. Leng, Active and deformable organic electronic devices based on conductive shape memory polyimide, ACS Appl. Mater. Interfaces 12 (2020) 23236–23243.
[42] R. Gupta, K.D.M. Rao, S. Kiruthika, G.U. Kulkarni, Visibly transparent heaters, ACS Appl. Mater. Interfaces 8 (2016) 12559–12575.
[43] T.J. Kang, T. Kim, S.M. Seo, Y.J. Park, Y.H. Kim, Thickness-dependent thermal resistance of a transparent glass heater with a single-walled carbon nanotube coating, Carbon 49 (2011) 1087–1093.
[44] H. Jang, S.K. Jeon, S.H. Nahm, The manufacture of a transparent film heater by spinning multi-walled carbon nanotubes, Carbon 49 (2011) 111–116.
[45] Y.H. Yoon, J.W. Song, D. Kim, J. Kim, J.K. Park, S.K. Oh, C.S. Han, Transparent Film Heater Using Single-Walled Carbon Nanotubes, Adv. Mater. 19 (2007) 4284–4287.
[46] D. Jung, D. Kim, K.H. Lee, L.J. Overzet, G.S. Lee, Transparent film heaters using multi-walled carbon nanotube sheets, Sens. Actuators A 199 (2013) 176–180.
[47] B. Zhou, X. Han, L. Li, Y. Feng, T. Fang, G. Zheng, B. Wang, K. Dai, C. Liu, C. Shen, Ultrathin, flexible transparent Joule heater with fast response time based on single-walled carbon nanotubes/poly(vinyl alcohol) film, Compos. Sci. Technol. 183 (2019) 107796.
[48] J. Kang, H. Kim, K.S. Kim, S. Lee, S. Bae, J. Ahn, Y. Kim, J. Choi, B.H. Hong, High-performance graphene-based transparent flexible heaters, Nano Lett. 11 (2011) 5154–5158.
[49] D. Sui, Y. Huang, L. Huang, J. Liang, Y. Ma, Y. Chen, Flexible and transparent electrothermal film heaters based on graphene materials, Small 7 (2011) 3186–3192.
[50] T.L. Chen, D.S. Ghosh, M. Marchena, J. Osmond, V. Pruneri, Nanopatterned graphene on a polymer substrate by a direct peel-off technique, ACS Appl. Mater. Interfaces 7 (2015) 5938–5943.
[51] G.H. Kim, J.H. Shin, T. An, G. Lim, Junction-free flat copper nanofiber network-based transparent heater with high transparency, high conductivity, and high temperature, Sci. Rep. 8 (2018) 13581.
[52] W. Lan, Y. Chen, Z. Yang, W. Han, J. Zhou, Y. Zhang, J. Wang, G. Tang, Y. Wei, W. Dou, Q. Su, E. Xie, Ultraflexible transparent film heater made of Ag nanowire/PVA composite for rapid-response thermotherapy pads, ACS Appl. Mater. Interfaces 9 (2017) 6644–6651.
[53] S.B. Singh, Y. Hu, T. Kshetri, N.H. Kim, J.H. Lee, An embedded-PVA@Ag nanofiber network for ultra-smooth, high performance transparent conducting electrodes, J. Mater. Chem. C 5 (2017) 4198–4205.
[54] J. Lee, J. Lee, S. An, D. Kim, T. Kim, S.S. Al-Deyab, A.L. Yarin, S.S. Yoon, Highly flexible, wearable stretchable, patternable and transparent heaters on complex 3D surfaces formed from supersonically sprayed silver nanowires, J. Mater. Chem. A 5 (2017) 6677–6685.
[55] Q. Huang, W. Shen, X. Fang, G. Chen, J. Guo, W. Xu, R. Tan, W. Song, Highly flexible and transparent film heaters based on polyimide films embedded with silver nanowires, RSC Adv. 5 (2015) 45836–45842.
[56] T. Kim, Y.W. Kim, H.S. Lee, H. Kim, W.S. Yang, K.S. Suh, Uniformly interconnected silver-nanowire networks for transparent film heaters, Adv. Funct. Mater. 23 (2013) 1250–1255.
[57] J. Lee, Y. Kim, H. Kim, H. Kim, C. Hong, Effect of AlOx protection layer on Ag-NWs for flexible transparent heater, Sci. Rep. 10 (2020) 4592.
[58] H. Seok, J. Kim, H. Kim, Effective passivation of Ag nanowire network by transparent tetrahedral amorphous carbon film for flexible and transparent thin film heaters, Sci. Rep. 8 (2018) 13521.
[59] Z. Lu, C. Yao, F. Xie, L. Si, F. Jia, J. Huang, Y. Wang, Q. Ma, Highly flexible and conductive sodium carboxymethyl cellulose/silver nanowires composite films, J. Mater. Sci. Mater. Electron. 31 (2020) 2353–2359.
[60] H. Yang, S. Bai, X. Guo, H. Wang, Robust and smooth UV-curable layer overcoated AgNW flexible transparent conductor for EMI shielding and film heater, Appl. Surf. Sci. 483 (2019) 888–894.
[61] Y. Huang, Y. Tian, C. Hang, Y. Liu, S. Wang, M. Qi, H. Zhang, J. Zhao, Self-limited nanosoldering of silver nanowires for high-performance flexible transparent heaters, ACS Appl. Mater. Interfaces 11 (2019) 21850–21858.
[62] R. Gupta, S. Walia, M. Hösel, J. Jensen, D. Angmo, F.C. Krebs, G.U. Kulkarni, Solution processed large area fabrication of Ag patterns as electrodes for flexible heaters, electrochromics and organic solar cells, J. Mater. Chem. A 2 (2014) 10930–10937.
[63] R. Gupta, K.D. Rao, K. Srivastava, A. Kumar, S. Kiruthika, G.U. Kulkarni, Spray coating of crack templates for the fabrication of transparent conductors and heaters on flat and curved surfaces, ACS Appl. Mater. Interfaces 6 (2014) 13688–13696.
[64] S. Xie, T. Li, Z. Xu, Y. Wang, X. Liu, W. Guo, A high-response transparent heater based on a CuS nanosheet film with superior mechanical flexibility and chemical stability, Nanoscale 10 (2018) 6531–6538.
[65] Z. Hefei, Z. Xiaoyang, L. Hongke, L. Hongbo, Fabrication of the large-area flexible transparent heaters using electric-field-driven jet deposition micro-scale 3D printing, Adv. Opt. Mater. 8 (2019) 527–533.
[66] J.S. Park, Y. Song, D. Park, Y. Kim, Y.J. Kim, Flexible transparent conducting films with embedded silver networks composed of bimodal-sized nanoparticles for heater application, Nanotechnology 29 (2018) 255302.
[67] S. Feng, S. Cao, Z. Tian, H. Zhu, D. Kong, Maskless patterning of biodegradable conductors by selective laser sintering of microparticle inks and its application in flexible transient electronics, ACS Appl. Mater. Interfaces 11 (2019) 45844–45852.
[68] Y. Li, Y. Chen, N. Tai, Highly thermal conductivity and infrared emissivity of flexible transparent film heaters utilizing silver-decorated carbon nanomaterials as fillers, Mater. Res. Express 1 (2014) 25605.
[69] S. Ji, W. He, K. Wang, Y. Ran, C. Ye, Thermal response of transparent silver nanowire/PEDOT:PSS film heaters, Small 10 (2014) 4951–4960.
[70] J.S. Woo, J.T. Han, S. Jung, J.I. Jang, H.Y. Kim, H.J. Jeong, S.Y. Jeong, K. Baeg, G. Lee, Electrically robust metal nanowire network formation by in-situ interconnection with single-walled carbon nanotubes, Sci. Rep. 4 (2014) 4804.
[71] D. Kim, L. Zhu, D. Jeong, K. Chun, Y. Bang, S. Kim, J. Kim, S. Oh, Transparent flexible heater based on hybrid of carbon nanotubes and silver nanowires, Carbon 63 (2013) 530–536.
[72] X. Li, S. Yu, L. Zhao, M. Wu, H. Dong, Hybrid PEDOT:PSS to obtain high-performance Ag NW-based flexible transparent electrodes for transparent heaters, J. Mater. Sci. Mater. Electron. 31 (2020) 8106–8115.
[73] L. Li, S.K. Hong, Y. Jo, M. Tian, C.Y. Woo, S.H. Kim, J. Kim, H.W. Lee, Transparent, flexible heater based on hybrid 2D platform of graphene and dry-spun carbon nanotubes, ACS Appl. Mater. Interfaces 11 (2019) 16223–16232.
[74] P.K. Kim, S. Chung, T. Ha, K. Jung, Transparent flexible heater with nano amorphous pattern, J. Micromech. Microeng. 29 (2019) 115010.
[75] P. Li, Y. Han, W. Wang, Y. Liu, P. Jin, J. Leng, Novel programmable shape memory polystyrene film: a thermally induced beam-power splitter, Sci. Rep. 7 (2017) 44333.